# *Fatigue Testing and Characterization of Pre-hydrided Zircaloy-4 Cladding Tubes*

## Nuclear Technology Research and Development


***Prepared for***
***U.S. Department of Energy***
***Advanced Fuels Campaign***
***Hong Wang, Paul Cantonwine, Yadu Sasikumar, Joshua Summers, Yong Yan, Nathan Capps, Kory Linton***
***Oak Ridge National Laboratory***



***Date: Aug. 29, 2024***
***ORNL/TM-2024/3512***
**M3FT-24OR0202020412**


**DISCLAIMER**

This information was prepared as an account of work sponsored by an agency of the U.S. Government. Neither the U.S. Government nor any agency thereof, nor any of their employees, makes any warranty, expressed or implied, or assumes any legal liability or responsibility for the accuracy, completeness, or usefulness, of any information, apparatus, product, or process disclosed, or represents that its use would not infringe privately owned rights. References herein to any specific commercial product, process, or service by trade name, trade mark, manufacturer, or otherwise, does not necessarily constitute or imply its endorsement, recommendation, or favoring by the U.S. Government or any agency thereof. The views and opinions of authors expressed herein do not necessarily state or reflect those of the U.S. Government or any agency thereof.

# SUMMARY

The solubility of hydrogen in Zircaloy-4 (Zry-4) at the cladding operating temperature is near 100 wt. ppm. Above this solubility limit, excess hydrogen precipitates as δ-hydride platelets in the cladding material. Because of the effect of the thermal gradient across the cladding thickness on the migration and precipitation of hydrogen, hydride rims are often observed at the cladding outer surface; under excessive corrosion conditions hydride blisters are possible. It is well known that the fatigue of metal alloys, especially high cycle fatigue, is sensitive to the status of surface including the microstructure, roughness, and residual stress. Thus, the question considered herein, is whether excessive hydrogen pickup modifies the microstructure such that it has a degradation effect on the fatigue performance of cladding during operation.

This report describes the evaluation of fatigue performance of a pre-hydrided Zry-4 cladding. A commercial Zry-4 was polished and pre-hydrided to 800 ppm and 1300 ppm H contents. The fatigue testing was conducted under strain control at 5 Hz with fully-reversed bending by using a cyclic integrated reversible bending fatigue tester (CIRFT). Six specimens with 1300 ppm and one specimen with 800 ppm were tested. Significant variation in test results were observed. While two of the 1300 ppm specimens failed with less than $1 \times 10^5$ cycles (at 0.32% and 0.41%), the four other samples did not fail over the strain amplitude range of 0.25% to 0.38%. Interestingly, the fracture initiation site of the failed samples was on the outside diameter (OD) surface rather than on the inside diameter (ID) surface as is typical for the as-polished cladding. This suggested a degrading effect of the hydriding process. Subsequently, three of the unfailed specimens were then further tested at ~0.43% to observe where failure initiation occurred. Significant variation was also observed in these three specimens. One specimen failed at ~9000 cycles while the two others failed at 43000 and $1.06 \times 10^5$ cycles. The performance here correlated to the location of failure initiation; failure initiated on the OD in the sample that failed after 9000 cycles while it initiated on the ID in the sample that failed after 43000 and $1.06 \times 10^5$ cycles. Flat features at the OD initiation sites suggest a brittle hydride feature on the surface of those samples was the cause of the degradation in fatigue performance, though the overall hydrogen levels in all samples was similar. A summary of all the observations is provided below:

- The un-failed specimens with 1300 ppm H were cycled to failure with a higher amplitude near 0.43%. In addition, the fatigue-treated specimen tended to have a longer fatigue at the same induced amplitude.
- Fractography revealed a mixed failure mode for the pre-hydrided specimen. Particularly, the specimen with fracture initiation site (FIS) located on the outer diameter surface of tube tended to have a shorter fatigue life than that of FIS on the inner diameter surface.
- Etched cross section was shown to have hydride platelets aligned with tube longitudinal axis as expected, and the density of hydrides is at the similar level as in literature data. Meanwhile, a LECO procedure was applied for hydrogen concentration measurement, which showed the measured hydrogen contents are close to the nominal value.
- With the polished cladding tube as baseline, O'Donnell-Lager (O-L) analysis showed that a decrease of about 50% in reduction-of-area (RA) would be needed for the O-L fitting to the fatigue data of 1300 ppm cladding.

The suggestion for the next steps is provided.

# CONTENTS

# FIGURES

## TABLES

# ACRONYMS

| | |
|---|---|
| AFC | Advanced fuels campaign |
| ASTM | International (formerly American Society for Testing and Materials) |
| AT | Axial tension |
| ATF | Accident tolerant fuel |
| CIRFT | Cyclic integrated reversible bending fatigue tester |
| DBT | Ductile to brittle transition |
| DI | Deionized |
| DOE | US Department of Energy |
| FIS | Fracture initiation site |
| HELP | Hydrogen enhanced localized plasticity |
| HT | Hoop tension |
| ID | Inside diameter |
| LOCA | Loss of coolant accident |
| LVDT | Linear variable differential transformer |
| OD | Outside diameter |
| O-L | O'Donnell-Langer |
| ORNL | Oak Ridge National Laboratory |
| PCMI | Pellet cladding mechanical interaction |
| RA | Reduction of area |
| RIA | Reactivity initiated accident |
| RT | Room temperature |
| SEM | Scanning electron microscopy |
| SNF | Spent nuclear fuel |
| TEM | Transmission electron microscope |
| UTS | Ultimate tensile strength |
| XRD | X-ray diffraction |
| Zry-2 | Zircaloy-2 |
| Zry-4 | Zircaloy-4 |

# FATIGUE TESTING AND CHARACTERIZATION OF PRE-HYDRIDED ZIRCALOY-4 CLADDING TUBES

## 1. BACKGROUD

The solubility of hydrogen in Zircaloy-4 (Zry-4) at the cladding operating temperature is near 100 wt. ppm.[1] Above this solubility limit, excess hydrogen precipitates as δ-hydride platelets in the cladding material. Mean hydrogen content of about 200–800 wt. ppm is commonly observed in Zry-4 fuel claddings at burnup around 60 GWd/tU.

Owing to the crystallographic orientation of the cladding material, hydrides are oriented with their normal preferentially aligned with the tube radial direction, which are so called circumferential hydrides. Because of the effect of the thermal gradient across the cladding thickness on the migration and precipitation of hydrogen, hydride rims and blisters are often observed at the cladding outer surface. These brittle external layers act as nucleation sites for further crack propagation through the substrate. The macroscopic ductility of the material decreases with increasing the thickness of hydride rims or blisters, which crack at the onset of plastic yielding of the substrate. The fracture resistance of the cladding under the pellet-cladding mechanical interaction (PCMI) loading depends on both the depth of hydride rims or blisters and the ductility and crack growth resistance of the substrate. The former is expected to crack at the very beginning of the reactivity-initiated accident (RIA) transient.

During its service in a reactor, cladding typically experiences complicated stress conditions induced by external pressurized fluid, internal gas pressure, pellet–cladding interaction, hydrodynamical load, temperature fluctuation, and so on. Apparently, the cladding system is subjected to the cyclic fatigue because of the inherent dynamic characteristic of loadings. A cladding system must maintain a high level of structural integrity throughout its entire service period, including during normal operation conditions or even beyond-design-basis accidents. The fatigue damage needs to be evaluated and addressed appropriately, especially considering the embedded hydrides within the matrix.

An ongoing initiative is working to systematically test and evaluate the Cr-coated zirconium alloy as one of the accident-tolerant-fuel (ATF) concepts. It has been demonstrated that the Cr-coating reduces the oxidation and also the penetration of hydrogen into the substrate and mitigates the hydride-induced ductile-to-brittle transition in the ring compression testing.[2] The effect of hydriding on the mechanical fatigue of the Cr-coated Zircaloy cladding system remains to be one of the major subtasks. The work presented in this report is dedicated to the effect of hydrides on the un-coated zirconium alloy or Zry-4.

## 2. INTRODUCTION

### 2.1 Effect of Hydrogen Content or Hydride on Tensile Properties

The effect of hydrogen content on tensile properties of pre-hydrided Zircaloy has been investigated previously. Huang and Huang, 1994,[3] studied a commercial Zry-4 that was annealed and pre-hydrided with hydrogen content from 0 to 340 ppm. The tensile tests used sheet specimens whose gauge length and thickness were 40 mm and 2 mm, respectively; all the specimens were tested with the loading axis perpendicular to the rolling direction. The ultimate tensile strength (UTS) of the material has been observed to increase with increasing hydrogen content at temperatures from 25 to 300$^{o}$C; the increases depend on the temperature, and the maximum increase reached about 20% at 200$^{o}$C. At the same time,

both reduction of area (RA) and elongation were decreased with the hydrogen content; the maximum decreases of RA and elongation were about 13% at 25°C and 29% at 100°C, respectively. The strengthening effect is attributed to dispersion hardening of hydride in the matrix. The fractography revealed secondary cracks which coincide with hydride precipitate sites. The initiation of micro-cracks at the hydride has been shown to be attributed to plastic deformation of matrix. The failure thus occurs by linking up brittle cracks in the hydrides by the ductile failure of matrix. The failure apparently is related to the distribution and geometrical size of hydrides. For a given Zircaloy matrix, it is the hydride spacing that dominates the coalesces of cracks once the hydride length reaches a critical value.

In another study by Kim et al., 2006,[4] a commercial Zry-4 was examined that had been pre-charged with hydrogen content to 1000 ppm. The ring tension specimens were extracted from the cladding tube that had an outer diameter (OD) of 9.5 mm and a thickness of 0.57 mm. The ring specimen has a width of 1.7 mm and a gauge length of 2.11 mm; the tension was thus in the circumferential direction. At room temperature, the UTS of the material exhibited a general rise with the increasing hydrogen content, but it turned into a slightly decrease after 700 ppm. The maximum increase in the UTS reached about 9%. The ductility, on the other hand, varied but overall presented a decreasing trend with the increasing hydrogen content, depending on the loading rate. The decrease in ductility was lower at 0.01/sec than that at 1/sec; the maximum decrease was amounted to be about 36% at 600 ppm. It was considered that hydride induces a stress mismatch between the ‘brittle’ hydride and the ‘soft’ metal phase. Crack initiated by either the hydride–metal interface or the broken hydride would be linked with another crack located in an adjacent hydride, thus a brittle fracture propagates easily in the case of high hydrogen content. The rate effect of UTS and ductility responses is attributed to an increase of the internal friction of the mobile dislocation inside the metal matrix. However, the authors did not comment the decrease in UTS in the high hydrogen content end.

The tensile response of Zry-4 was symmetrically studied by Saux et al., 2010,[5] using various specimen geometrical shapes include axial tension (AT) and hoop tension (HT), in which the specimens were prepared from the cladding tubes. The cladding was cold-worked stress-relieved with an OD of 9.5 mm and a thickness of 0.57 mm, and pre-charged with hydrogen content as high as 1200 ppm. The gauge length and width of the AT specimen were 15 mm and 3 mm, respectively; those of HT were 3 mm and 2 mm, respectively. The tests were conducted at various temperatures. The variation of UTS was affected more by the temperature than specimen configuration. At the RT, there was a monotonic increase in UTS with the increasing hydrogen content, which was amounted to 7% at 1200 pm. On the other hand, the AT elongation maintained a flat response until 400 ppm, beyond which a decrease was observed with about 19% at 1200 ppm. The mechanical strengthening is commonly attributed to a composite reinforcement caused by hydrides (harder than the matrix at room temperature). The decrease in material strength for low hydrogen contents at 350°C and 480°C is probably due to a softening effect of the dissolved hydrogen. This softening is attributed to a decrease in the Zr–Zr bond order caused by solute hydrogen, to a decrease in the dislocation pinning caused by interstitial atoms and/or to the enhancement of dislocation mobility. The strengthening observed for high hydrogen contents reflects the hardening contribution of hydrides. This hardening is expected to decrease when temperature increases, as deformability of hydrides is increased.

The RT responses in UTS and RA and elongation as reviewed above were observed by Wang et al., 2013, on an annealed Zry-4 plate material.[6] The mini-tensile specimen had a gauge length of 10 mm, width of 3 mm and thickness of 2 mm; specimen was loaded perpendicularly to the rolling direction. The UTS showed a monotonic increase as a function of hydrogen content, with about 6% increase at 850 ppm. Both the RA and elongation exhibited significant losses with the hydride introduced. With hydrogen content increasing from 0 to 850 ppm, the RA decreased from 53% to 10% and the elongation from 30 % to 5%. One suggestion for this strengthening effect was that the hydrides precipitated in the Zircaloy-4 matrix

normally possessed higher strength than that of the surrounding matrix and hence acting as the reinforcing phase and resulting in the mechanical strengthening of the hydrided material. Another suggestion was that a large number of dislocations were generated in the α-Zr matrix during the hydride formation, contributing to the strengthening of hydrided Zry-4. The generation of the dislocations in the matrix is a consequence of the accommodation of the dilatational misfit strain associated with the hydride precipitation and has been evidenced by transmission electron microscope (TEM) investigations.

The effect of hydride on the mechanical properties of Zry-4 has been studied recently by Tung and Chen, 2024.[7] The sheet material was used, which was pre-charged with hydrogen content to 1217 ppm. The tensile specimen had a gauge length of 32 mm, width of 3 mm and thickness of 1.6 mm. The plots of UTS vs. hydrogen content at temperatures from 25 to 100°C generally are quite parallel. Most of the plots feature a slightly fall-and-rise fluctuation near 450 ppm, except at 25°C. The final increase in RT UTS was about 20% at 1217 ppm. A ductile to brittle transition (DBT) was revealed near 750 ppm for tests at 25 to 75°C. The overall decrease in RT RA was about 59%, while an abrupt decrease near 750 ppm accounting for 75% of the total decrease. The elongation exhibited also an apparent decrease with the increasing hydrogen content with a fluctuation observed near 450 ppm, corresponding to that observed for UTS. The final decrease in RT elongation at 1217 ppm was amounted about 77%. The strengthening effect with UTS is attributed to the role of precipitated hydrides, which act as impediments to dislocation motion, thereby increasing the material's strength. The phenomenon of hydrogen embrittlement in zircaloy can be elucidated through the concept of hydrogen-enhanced localized plasticity (HELP). It involves the enhancement of dislocation mobility by hydrogen, leading to localized slip bands in the material under stress, ultimately resulting in embrittlement.

The effect of hydride on the tensile properties has been experimentally studied also for Zry-4 in fully-recrystallized condition by Lee et al., 2020.[8] The Zry-4 was pre-hydrided as high as 1400 ppm. A sheet specimen was used with gauge length 25.4 mm, width 3.7 mm and thickness 0.5 mm; loading is also applied perpendicularly to the rolling direction. Contrary to the monotonic increase reviewed above, a two-stage RT UTS response was observed as a function of hydrogen content with a rise-and-fall near 500 ppm. Overall decrease in UTS attained as high as 26%. Accordingly, the RT elongation displayed a two-stage decrease as a function of hydrogen content with the transition point near 500 ppm. At 1200 ppm, the total elongation was fully consumed down to zero. The different work hardening behaviors as revealed by the two-stage UTS response can be explained with the effect of preferred basal orientations. Generally, residual stresses on hydride precipitations and dislocations generated from the hydride formation act as strengthen sources in the alloy. Variations were also reported because of complicated mechanical interactions between hydride and matrix. For instance, Lin et al., 1979,[9] observed slightly increases with hydrogen content until 400 ppm but decrease at higher hydrogen content. Bai et al., 1994,[10] also showed that hydrogen contents did not significantly influence the tensile strength in lower hydrogen content range, but in higher hydrogen content range the tensile strength tended to decrease. Bai et al. commented that precipitation generally induces hardening but hydride precipitation in Zr alloys may deplete hardening because tensile residual stresses such as micro-cracks around hydride precipitation developed in matrix.

### 2.1.1 Summary

The previous experimental work on the tensile property study is summarized in Table 1 with focus on the RT condition.

*Table 1 Literature data for RT tensile properties of Zry-4 with various hydride conditions*

| Zry-4 specimen | Hydrogen content | UTS variation | RA variation | Elongation variation | Refs. |
|---|---|---|---|---|---|
| Annealed. Sheet, 40 mm×2 mm | 300 ppm | 8% rise | 13% fall | 18% fall | Huang & Huang, 1994[3] |
| Ring. 2.11×1.7×0.57 $mm^3$ | 1000 ppm | 9% rise and fall near 750 ppm | | 36% fall | Kim et al., 2000[4] |
| AT, 15×3×0.57 $mm^3$ | 1200 ppm | 7% rise | | 19% fall | Saux et al., 2010[5] |
| Annealed. Sheet, 7.5×3×2 $mm^3$ | 850 ppm | 6% rise | 81% fall | 83% fall | Wang et al., 2013[6] |
| Sheet, 32×3×1.6 $mm^3$ | 1217 ppm | 20% rise | 59% fall | 77% fall | Tung & Chen, 2024[7] |
| Fully-recrystallized. Sheet, 25.4×3.7×0.5 $mm^3$ | 1400 ppm | 8% rise and fall near 500 ppm, 26% total fall. | | 100% fall | Lee et al., 2020[8] |

## 2.2 Effect of Hydrogen Content on Fatigue Performance

The effect of hydride on the mechanical fatigue of Zircaloy has been also part of the previous research, even relevant literature data is limited. In the work by Wanhill, 1968,[11] the sheet specimens with a gauge section of 50×12.7×2.5 $mm^3$ were extracted from a Zry-2 tube with the specimen length aligned with tube longitudinal axis. The specimens were annealed under hydriding condition at 400°C for 72 h at a hydrogen flow rate of 10 ppm/h. The tensile fatigue tests were conducted at 128 Hz with a stress ratio of R = 0.2 for the specimens of various hydrogen contents. Both RT and 300°C fatigue responses were examined. At the RT, un-hydrided specimens survived 3 to 6 $x10^7$ cycles at maximum stress of 345 MPa. While some of pre-hydrided specimens also survived more than 1 to $2x10^7$ cycles at the same stress, but failure was observed for those pre-hydrided 100 to 600 ppm, with a fatigue life of 1 to $5x10^6$ cycles. Therefore, the hydride affected the RT fatigue performance of Zry-2. With a R value of 0 to 0.1, the effect of hydride on the 300°C fatigue life of Zry-2 seemingly depended on stress amplitudes but was generally insignificant within the range of hydrogen contents tested.

## 2.3 Technical Gap and Approach

As suggested by the review above, the fatigue data of Zircaloy cladding tube related to hydride is quite limited. Lack of the relevant data presents a significant technical barrier to deploying of the identified ATF concepts such as Cr-coated Zry-4.

A cyclic integrated reversible bending fatigue tester (CIRFT) is proposed in the current study to test and characterize the fatigue response of Zry-4 cladding tubes in a range of strain amplitudes. 6-in Zry-4 cladding tubes were polished and then heat-treated under hydriding condition to a nominal hydrogen content of 800 ppm and 1300 ppm. In the following sections, the experimental approach, experimental results and discussion, conclusion and future work are provided.

# 3. EXPERIMENTAL METHODS AND MATERIALS

## 3.1 Test system and Data Processing

The CIRFT used in this study was developed for studying the vibration integrity of spent nuclear fuel (SNF) rods in a hot cell . The system is set up on a testing bench and uses a U-frame to convert the linear motion into bending moment in the rod specimen being tested. The linear motion is supplied by the dual linear motors aligned on the bench. The U-frame is made of two rigid arms with specially-designed specimen grips. The system measures the deformation of the rod by using three linear variable differential transducers (LVDTs) installed in the gauge section. Relevant detail of the system components, design considerations, and calibration can be found in previous publications.[12-18] Detail concerning the use of the system in testing a variety of SNF rods and relevant data can be found in additional references.[19-26] Recently, the CIRFT has been successfully utilized to test and characterize the fatigue response of cladding tube where no pellets are involved.[27] A schematic is provided in Fig. 1 to illustrate the arrangement of three LVDTs with respect to the bending rod; the deflections are designated as $d_1$, $d_2$, and $d_3$, and the sensor spacing is denoted as 'h'.

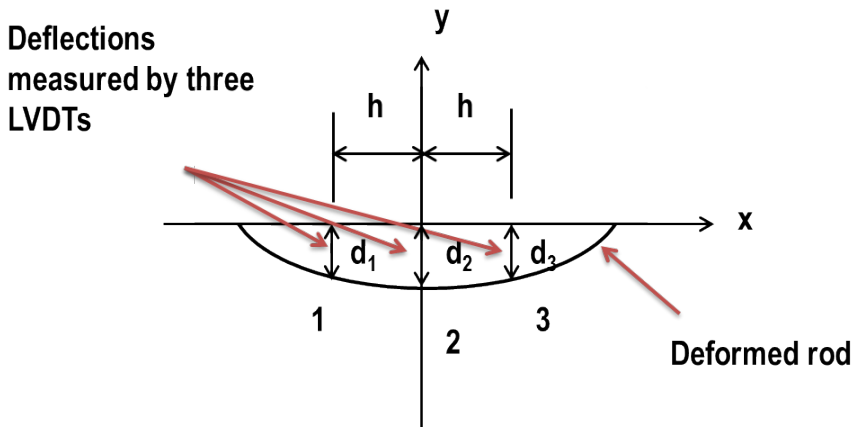


*Fig. 1 Schematic showing the curvature determination of a rod by using deflections measured at three points. The LVDTs are located on the convex side of the bending rod.*

The moment is calculated as

$$M = F \cdot L, \quad (1)$$

where $F$ is the averaged value of loads from the dual motors, and $L$ is the loading arm length of the U-frame. The curvature, κ, of the tube was estimated by using deflections $d_1$, $d_2$, and $d_3$ from three LVDTs. The calculation and correction of curvature can be found in related publications.[28,29] Time series in moment and curvature were obtained from online monitoring or measurement, which can be converted into a moment–curvature loop. The moment amplitude, or half moment range, ΔM/2, can be expressed in terms of peak $M_p^+$ and valley $M_p^-$, as follows:

$$M_a = \Delta M/2 = (M_p^+ - M_p^-)/2. \quad (2)$$

The curvature amplitude Δκ/2 of tube can be measured similarly by peak $\kappa_p^+$ and valley $\kappa_p^-$,

$$\kappa_a = \Delta\kappa/2 = (\kappa_p^+ - \kappa_p^-)/2. \quad (3)$$

Further characterization of tube response was performed by using flexural rigidity, R, and hysteresis, $U_M$, as defined by the following,

$$R = \Delta M/\Delta\kappa, \quad \text{and} \quad (4)$$

$$U_M = \oint M d\kappa. \quad (5)$$

The flexural hysteresis results from the damping of system, which measures the amount of energy dissipated in a cycle.[30,31]

Given the moment and curvature, the stress and strain amplitudes at the outer fiber of bending tube can be calculated by using beam theory:

$$\sigma_a = M_a y_{max}/I, \text{ and} \quad (6)$$

$$\varepsilon_a = \kappa_a y_{max}, \quad (7)$$

where $y_{max}$ is the outer radius of the tube, and $I$ is the area moment of inertia. Furthermore, the rigidity of tube can be calculated by

$$R = EI, \quad (8a)$$

where $R$ is given by Eq. (4). The elastic modulus of cladding tube substrate can be estimated as follows,

$$E = R/I. \quad (8b)$$

Flexural hysteresis $U_M$, Eq. (5), can be expressed in terms of loss angle, $\phi_R$, amplitudes of M-κ loop, or R for the curvature control fatigue as follows:

$$U_M = \pi R \kappa_a^2 \sin\phi_R, \quad (9)$$

which can be rewritten for the loss angle as

$$\phi_R = \sin^{-1}[U_M/\pi R \kappa_a^2]. \quad (10)$$

Similar expressions can be found for various physical systems such as mass-spring-damper, piezoelectrics and dielectrics.[31,32]

## 3.2 Materials and Specimen Preparation

The commercial cold-worked and stress-relieved Zry-4 cladding tubes were purchased from Cameco Fuel Manufacturing (Port Hope, Ontario, Canada). The chemical composition of Zry-4 is maintained within the range as specified by ASTM standard B353-12.[33] The Zry-4 cladding tube was polished by the vendor APEX with fine grinding. The polished tube was cut into 6" (152.4 mm) sections. Each section was then

treated with a hydriding procedure:[34] the sample was heated from 20°C to 450°C at 0.5°C/min, held at 450°C for 16 h, and then cooled down to RT at 1°C/min. The nominal hydrogen content was 1300 ppm. In addition, a couple of cladding tube was pre-hydrided to 800 ppm to examine the trend of fatigue life against the hydrogen content. The hydriding treatment condition in this study approaches that of stress relief as discussed in Fourgeaud et al., 2009[35] and thus offers additional annealing effect.

The tube specimen was obtained by cutting a 4" (101.6 mm) section from the supplied pre-hydrided tube and then assembled into two rigid endcaps by using epoxy bonding; the assembly diagram is shown in Fig. 2. The specimen had an overall length of 152.4 mm with a gauge section of 50.80 mm. The pre-hydrided tubes had ODs between 9.22 and 9.31 mm; inner diameters (IDs) were varied between 8.25 and 8.44 mm. Six specimens were prepared for 1300 ppm, and two for 800 ppm.

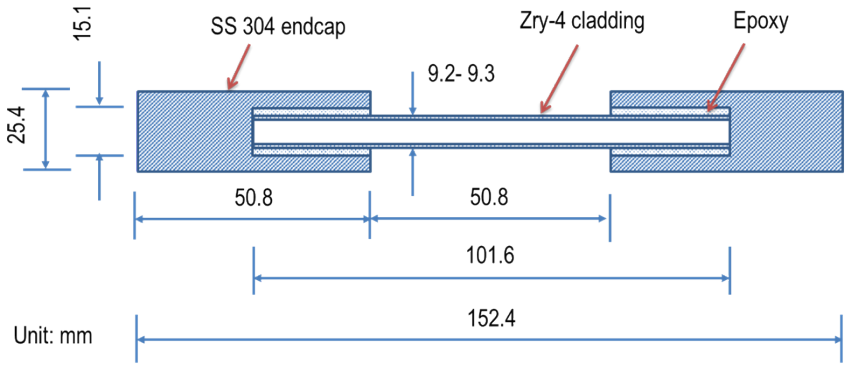


*Fig. 2 Schematic for specimen assembly used in fatigue testing.*

## 3.3 Test Procedure

Fatigue tests were conducted under fully reversed (R = −1) bending at RT. A typical test consists of test sessions; each involves a measurement step with 0.05 Hz and low amplitude and a cycling step at 5 Hz with target amplitude for specified number of cycles. 5 Hz cycling was conducted under displacement control; the input was designed to cover a range of expected fatigue lives. Each session had a target number of cycles, such as 10k, 90k, 200k, and so on. The test proceeds until the specimen fails or the test is interrupted. The strain based on the deflections of specimens at the three points was calibrated against strain measurement with a strain gage mounted on a reference tube specimen. The deflections and equivalent strain were monitored and evaluated in cycling. Thus, the fatigue testing is equivalent to that of strain control. The fracture surface was studied on selected specimens for each cladding condition using scanning electron microscope (SEM). The study focused on the fracture initiation site and fatigue failure mechanism involved. The related procedures are established elsewhere and can be found in the literature.[28,36-40]

# 4. EXPERIMENTAL RESULTS

Fatigue testing was carried for 1300 ppm group under induced strain amplitude range from 0.25% to 0.41% with the number of cycles ranged from $1.06\times10^4$ to $3.27\times10^6$. Only two specimens, H101 and H103, were cycled to failure with fatigue lives of $1.06\times10^4$ at 0.41% and $4.90\times10^4$ at 0.32%, respectively. Rest survived $1.0\times10^6$ to $3.27\times10^6$ cycles at strain amplitudes between 0.32% and 0.38%. One fatigue test was conducted for 800 ppm group, H201, which survived $3.11\times10^6$ cycles at 0.37% amplitude. It has been decided to hold off the fatigue testing on 800 ppm group and to focus on the un-failed 1300 ppm specimens. Thus, the following discussion is concentrated on the work with 1300 ppm group, even though the data with 800 ppm are presented along.

H102, H105, and H106 were selected in the second round of testing but with a higher strain amplitude near 0.43%. These specimens, re-named as H301 to H303, were finally cycled to failure in the repeated tests with fatigue lives ranged from $9.2\times10^4$ to $1.06\times10^5$. A summary of fatigue test conditions and main results is provided in Table 2.

*Table 2 Main fatigue results, 5Hz, fully-reversed.*

| $H_C$ | Spec | Spec1 | $d_a$ | $\kappa_a$ | $\varepsilon_a$ | N or $N_f$ | Fail | ID | OD |
|---|---|---|---|---|---|---|---|---|---|
| ppm | | | mm | $m^{-1}$ | % | Cycles | | mm | mm |
| 1300 | H103 | | 3.38 | 0.89 | 0.41 | 10,600 | 1 | 8.437 | 9.311 |
| 1300 | H101 | | 2.4 | 0.69 | 0.32 | 49,000 | 1 | 8.237 | 9.279 |
| 1300 | H104 | | 2.25 | 0.70 | 0.32 | 1,004,000 | 0 | 8.303 | 9.247 |
| 1300 | H105 | | 2.8 | 0.82 | 0.38 | 3,001,000 | 0 | 8.386 | 9.274 |
| 1300 | H106 | | 2.82 | 0.82 | 0.38 | 3,109,000 | 0 | 8.336 | 9.223 |
| 1300 | H102 | | 2.1 | 0.55 | 0.25 | 3,270,000 | 0 | 8.247 | 9.274 |
| 800 | H201 | | 2.6 | 0.81 | 0.37 | 3,106,000 | 0 | 8.344 | 9.246 |
| 1300 | H302 | H102 | 3.45 | 0.94 | 0.43 | 9,200 | 1 | 8.247 | 9.274 |
| 1300 | H301 | H105 | 3.41 | 0.93 | 0.43 | 43,000 | 1 | 8.386 | 9.274 |
| 1300 | H303 | H106 | 3.44 | 0.96 | 0.44 | 106,000 | 1 | 8.336 | 9.223 |

Note: $H_c$ – hydrogen content; H1xx –1300 ppm group; H2xx –800 ppm group; H3xx- 1300 ppm group fatigue-treated to more than $3\times10^6$ cycles; xx- specimen number. Spec1 – original specimen label; $d_a$ – displacement amplitude for the single linear motor.

## 4.1 Moment and Curvature

Both moment and curvature varied during cycling as a response of cycling as shown in Fig. 3 (a) and (c). Moment amplitudes were usually pretty stable during cycling. H103 was exceptional and the moment appeared quite dynamic when it was approaching failure, which was consistent with the fast increase of curvature. For those failed, H101 and H103, the specimens generally exhibited a rising trend of curvature. The fatigue curve of curvature of H102 had a downward movement prior to the interrupt of cycling. The complicated response should be attributed to the material because the deflection curves showed a similar trend. The measurement data at 0.05 Hz also indicated a decrease trend of curvature with the number of cycles accumulated. It remains to examine if it is due to the recovery of material due to the intersession.

The scatter plot of averaged moments and curvatures as a function of number of cycles to failure is shown in Fig. 3 (b) and (d) along with the previous data related to the as-received (AR) and polished Zry-4 cladding tubes.[41] Because polishing used in the current study had a procedure same as before, the comparison can be made between the hydrided and polished data groups for the evaluation of effect of hydride. In the low cycle region, the two failure data points for 1300 ppm group are located towards the lower-left side of previous data in both M-N and k-N plots. The 1300 ppm data in the high cycle regions display a large data band, especially in k-N plot. Meanwhile, a wide variation of fatigue life was observed for the 1300 ppm specimens that were fatigue-treated. H301 and H303 even had a longer fatigue life than those of as-received and polished specimens at the same curvature amplitude.

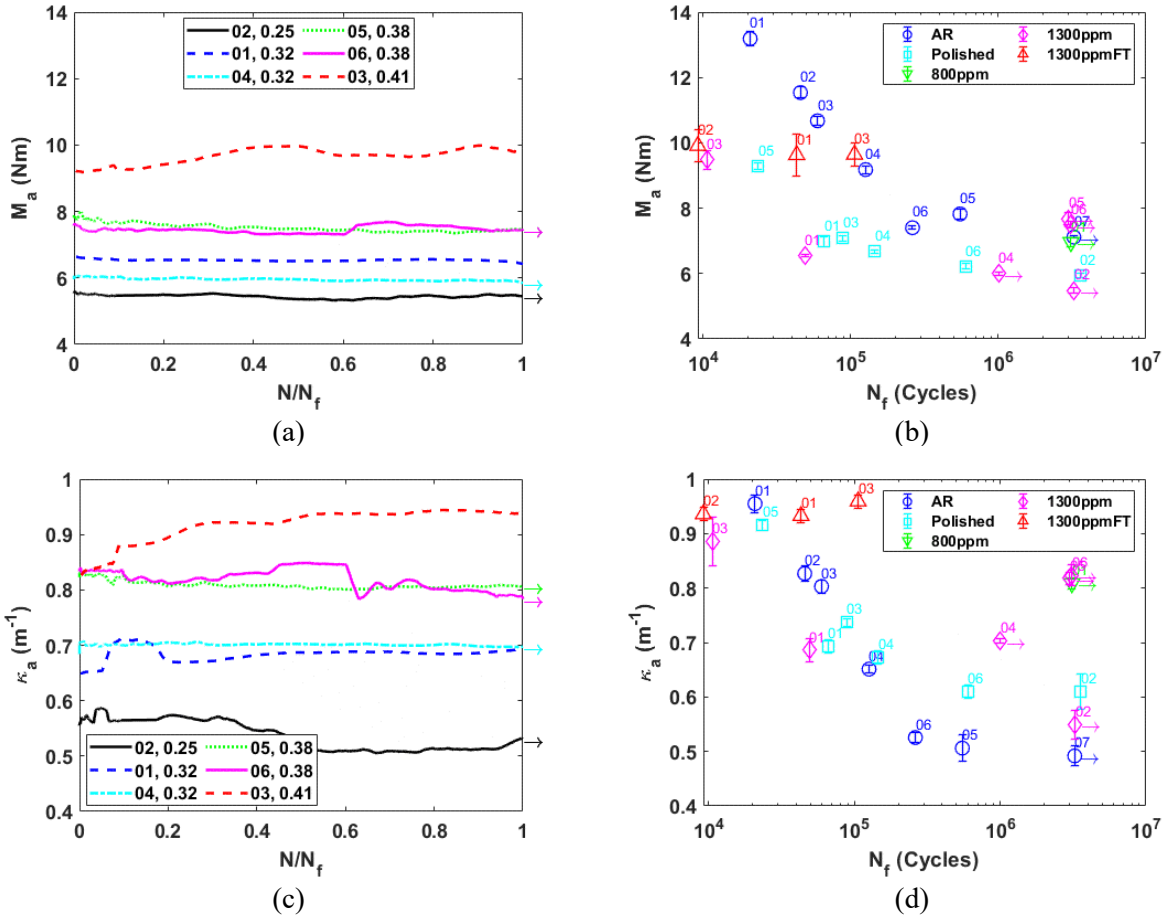


*Fig. 3 (a) and (c)Moment and curvature as a function of the normalized number of cycles for H1 group ($N_t$ – total cycles); (b) and (d) are the averaged quantities where the data of as-received and polished un-hydrided specimens are included for comparison. Legend "xx ,yy" in (a) and (c) has following meanings: xx-specimen number, yy-strain amplitude in %; legend with 1300ppmFT in (b) and (d) represents the 1300 ppm specimen fatigue-treated to > $3\times10^6$ cycles; the error-bar represents one standard deviation. Arrow indicates the test interrupted. Same comments apply in the following.*

## 4.2 Flexural Rigidity and Hysteresis

The fatigue curves and scatter plots of rigidity and hysteresis are presented in Fig. 4. For the failed specimens, fatigue curves demonstrate that: 1) flexural rigidity decreased in general, and 2) hysteresis increased. H102 and H106 again exhibited distinct behavior with a rising R curve, while the hysteresis was largely flat with a slightly tendency to decrease with the normalized number of cycles.

In general, the R values of pre-hydrided specimens are fairly close to but a little lower than those of the polished, which is consistent with the procedure used in hydriding in both polishing and heat treatment. The data points of failed specimens on the hysteresis scatter plot are located leftwards from the rest of database. In the high cycle region, the induced hysteresis had with a wide variation range but scattered around the averaged level of previous results.

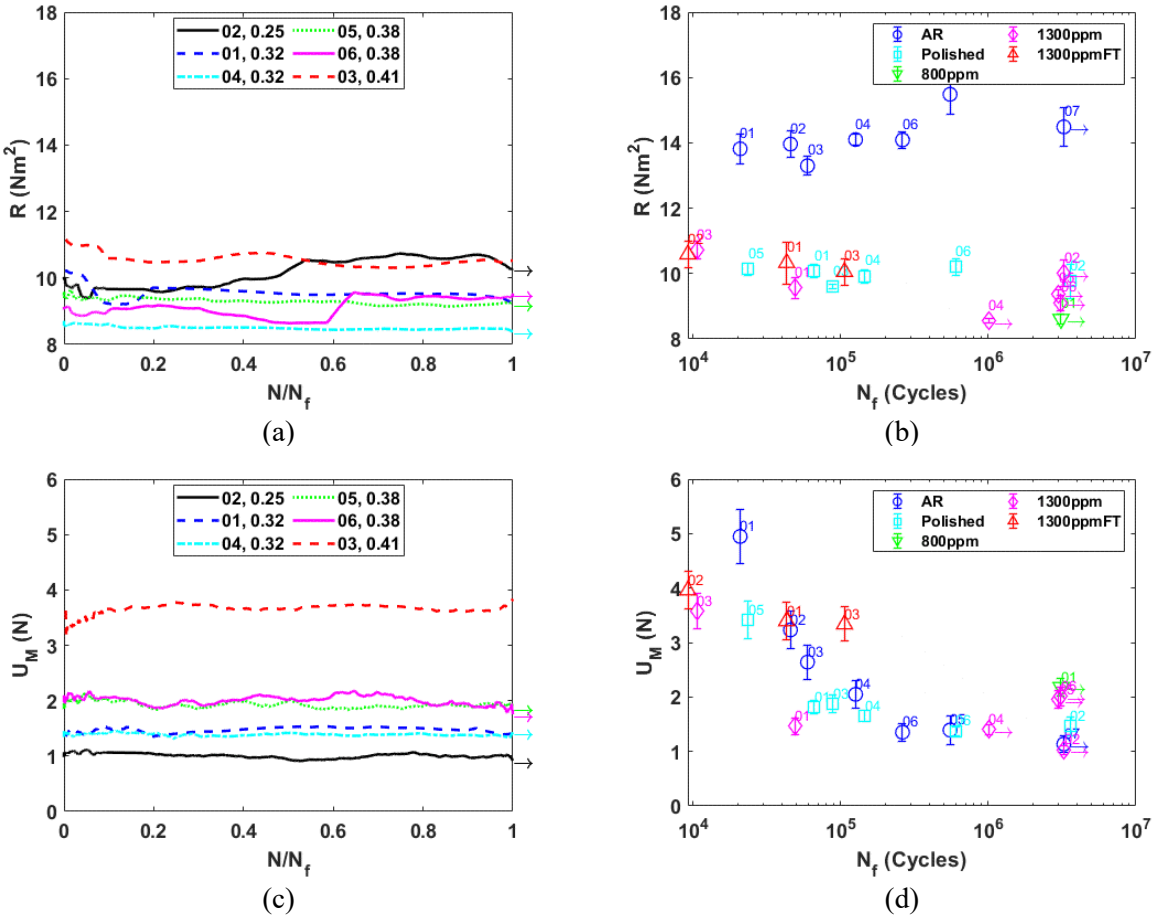


*Fig. 4 (a) and (c) Flexural rigidity and hysteresis as a function of $N/N_f$ for H1 group; (b) and (d) averaged quantities where the data of as-received and polished un-hydrided specimens are included for comparison.*

## 4.3 Equivalent Quantities

### 4.3.1 Stress and Strain

The equivalent stress and strain on the outer fiber of bending rod were estimated. The results are characterized in terms of averaged values and shown in Fig. 5. The stress and strain responses of pre-hydrided cladding materials generally reflect those observed for the curvature and moment as illustrated above. All the data points of pre-hydrided cladding material are seen located below or within the data zone of previous results in the σ-N plot.

In the high cycle region, the induced strain amplitudes for the pre-hydrided un-failed specimens H104 to H106 are seen quite above the main body of database on the ε-N plot. In the low cycle region, the data points are located toward the lower-left side of the previous data. The repeated fatigue testing on the un-failed specimens at high amplitude indeed resulted in the failure. It appeared that the fatigue-treated specimens like H301 and H303 tended to display a fatigue life aligned with the as-received and polished groups. It remains to confirm, for the pre-hydrided to 1300 ppm group of cladding material, if there is a substantial difference in micro-structures between the outstanding specimens and other specimens tested.

It shall be pointed out that the fatigue response of pre-hydrided Zry-4 cladding tube agrees with the previous observations with the effect of hydriding on mechanical properties as reviewed above. The reduction of the RT RA of Zry-4 with hydrogen content as reported by majority of literature data corresponds to a reduced fatigue life in the low cycle range observed in the current study. The stable or increase in the RT UTS as related to the strengthening of hydrides as revealed by the previous studies, on the other hand, suggests that the RT fatigue limit of pre-hydrided Zry-4 tends to be higher than that of the un-hydrided cladding tube, which is validated by the current study. The quantification of the relevant effect obviously needs more data analysis.

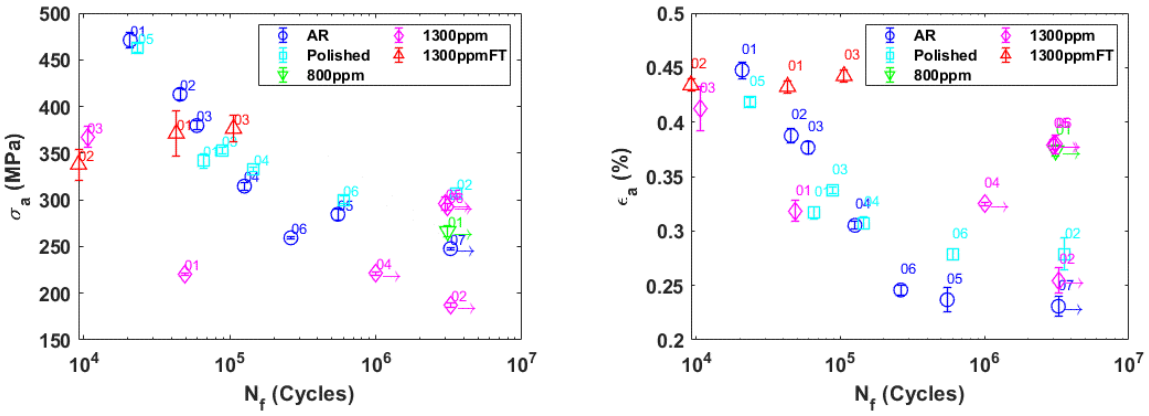


(a) (b)

*Fig. 5 (a) Stress and (b) strain as a function of the number of cycles to failure. AR – as-received; 1300ppmFT- pre-hydrided to 1300 ppm and cycled to more than $3\times10^6$ cycle.*

### 4.3.2 Modulus and Loss Angle

Young's modulus and loss angle of pre-hydrided specimens were extracted and the results are presented in Fig. 6. While the loss angles fall within the data zone of previous results, the pre-hydrided specimens displayed a modulus much lower than other Zry-4 specimens tested including those of the as-received and polished. The decrease in Young's modulus due to pre-hydriding accounts for about 25%. The similar decrease in Young's modulus with pre-hydrided Zry-4 cladding was also reported by Lee et al., 2020,[8] who suggested that the decrease in Young's modulus was partly arising from the embrittlement of the hydride and the effect of micro-cracks in hydrides. It is believed that the mis-matched stress in hydride-matrix interface may induce the additional structural damage that compromises the modulus. Meanwhile, the heat-treatment in hydriding process annealed the cladding tube, while the subsequent cyclic treatment introduced hardening. On the other hand, compared to those of polished specimens, the loss angle of the pre-hydrided specimens showed a relatively low value, especially in the high cycle region, but the difference appears to be statistically insignificant.

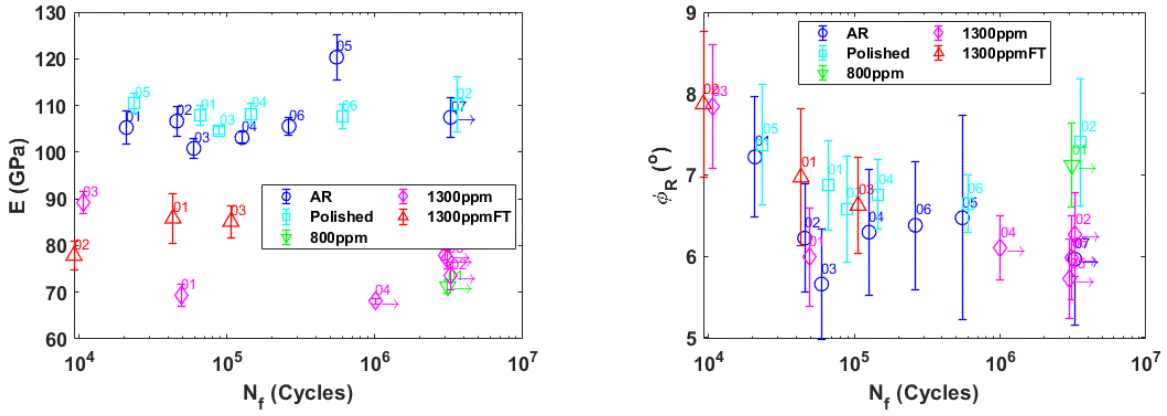


(a) (b)

*Fig. 6 (a) Young's modulus, and (b) loss angle as a function of the number of cycles to failure.*

# 5. FRACTOGRAPHICAL ANALYSIS AND HYDROGEN MEASUREMENT

## 5.1 Pictures of Post-tested Specimens

Failure of the tested and failed specimens mostly took place in the gauge section of specimens. The failure position of H302 occurred on the edge of endcap, but it is still considered as an effective data point for the reason discussed previously.[16] Three failures were located away from LVDTs (H101, H103, H303) and two were facing the LVDTs (H301, H302), the pictures of which for the tested H101 and H103 are shown below Fig. 7. The examination of failure positions of failed specimens on the ε-N scatter plot in Fig. 5 (b) did not reveal any correlation between the two.

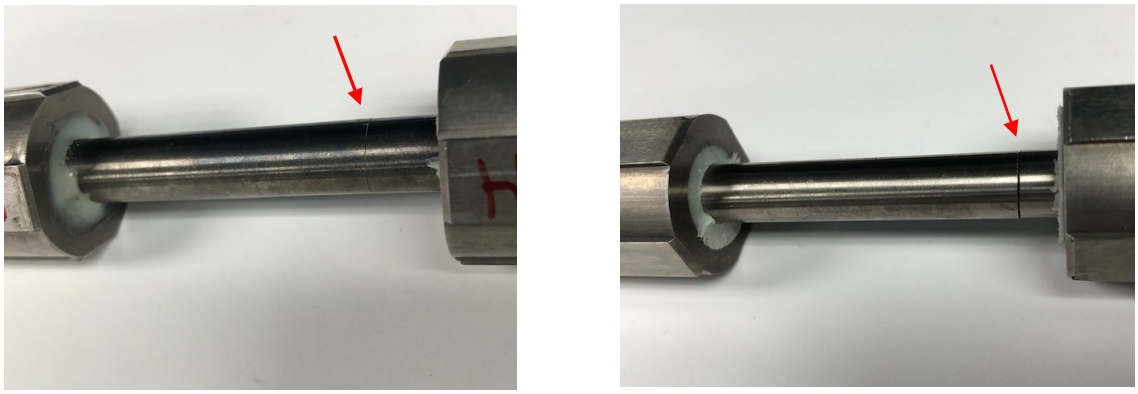

(a) (b)

*Fig. 7 (a) H101 fracture initiated from surface away from LVDTs; (b) H103 fracture also initiated from surface away from LVDTs.*

## 5.2 Fractography

The fracture cross sections of fatigue-failed samples (H101, H103, H301 to H303) were characterized to study the fracture initiation sites (FIS) using SEM on a TESCAN MIRA 3 Field Emission Microscope. All samples showed poorly resolved fatigue striations and black arrow marks have been overlayed to show the direction of crack propagation from the FIS identified. Rubbing defects were observed in and

around the initiation site in sample H302, potentially from the interaction of the Zry-4 and the epoxy used to hold the sample in the fixtures.

The FISs of samples H101 to H302 are shown in Fig. 8 to Fig. 11, respectively. The fracture is seen to have initiated on the OD side of the sample and propagated inwards towards the inner diameter (ID) in samples H101, H103 and H302. On the contrary, in samples H301 and H303, the fracture is observed to have initiated on the ID and at a localized defect site, as shown in the high magnification insert in Fig. 10 for H301.

No localized surface defects were observed, as the source of fracture initiation, in samples that failed on the OD. However, smooth region was observed in these samples on the crack initiation site with striations similar to fatigue striations. This flat region, shown in the high magnification inserts in Fig. 8, resembles a macroscopic δ-hydride packet like structure shown by Chung et al.[42] Although the presence of this hydride-rim-like feature justifies the (preferential) crack initiation location due to its significant influence in the blunting and sharpening processes,[43] more analysis is required to conclusively identify this feature.

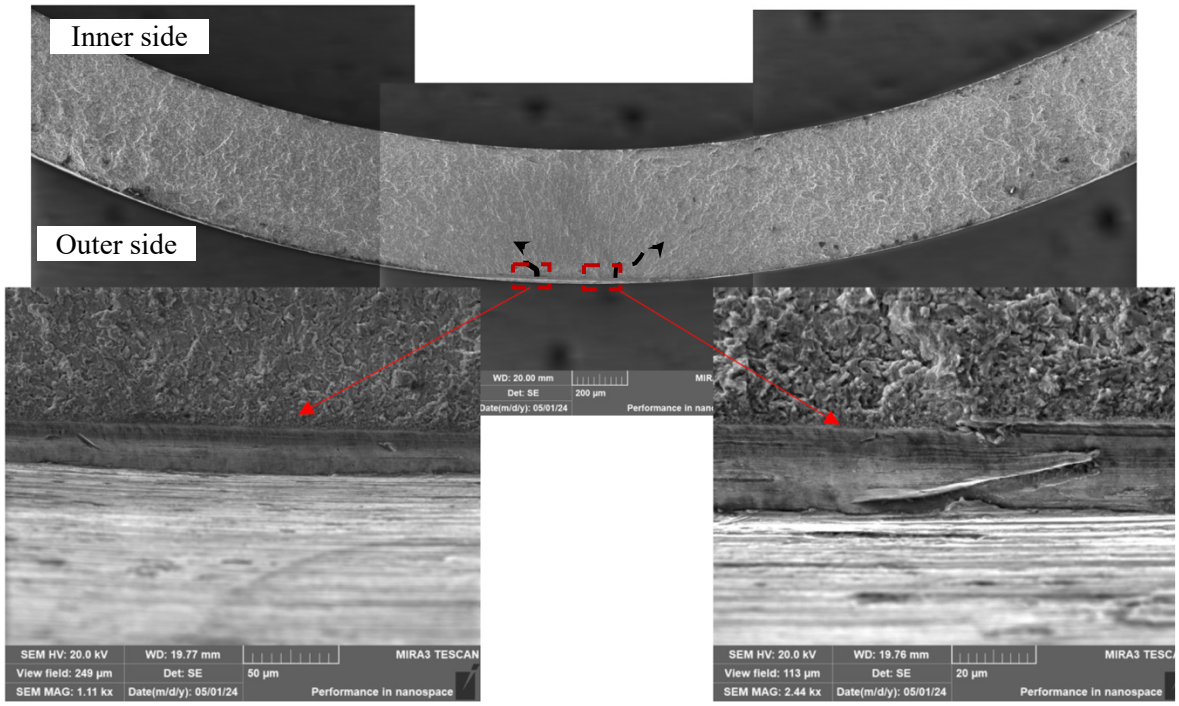


*Fig. 8. High magnification images showing features on the crack initiation site of sample H101. Black dashed arrows indicate the direction of crack propagation from the initiation site.*

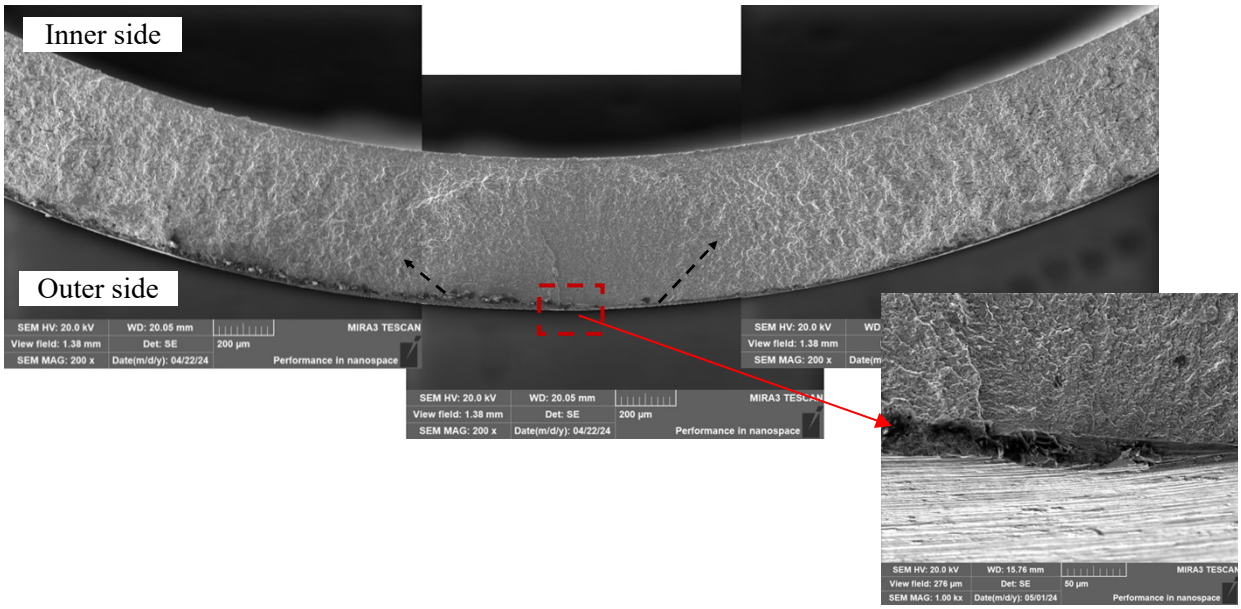


*Fig. 9. Fracture initiation site of sample H103. Insert shows a high magnification image of features on the crack initiation site. Black dashed arrows indicate the direction of crack propagation from the initiation site.*

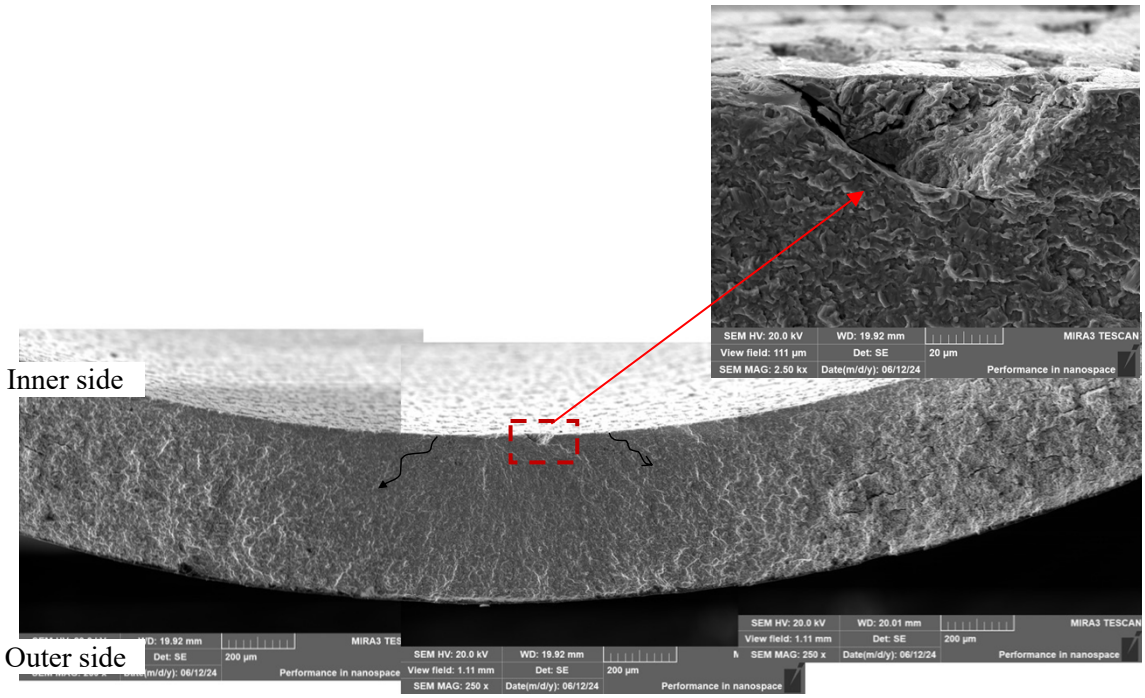


*Fig. 10. Fracture initiation site of sample H301. Insert shows a high magnification image of the crack initiation site. Black arrows indicate the direction of crack propagation from the initiation site.*

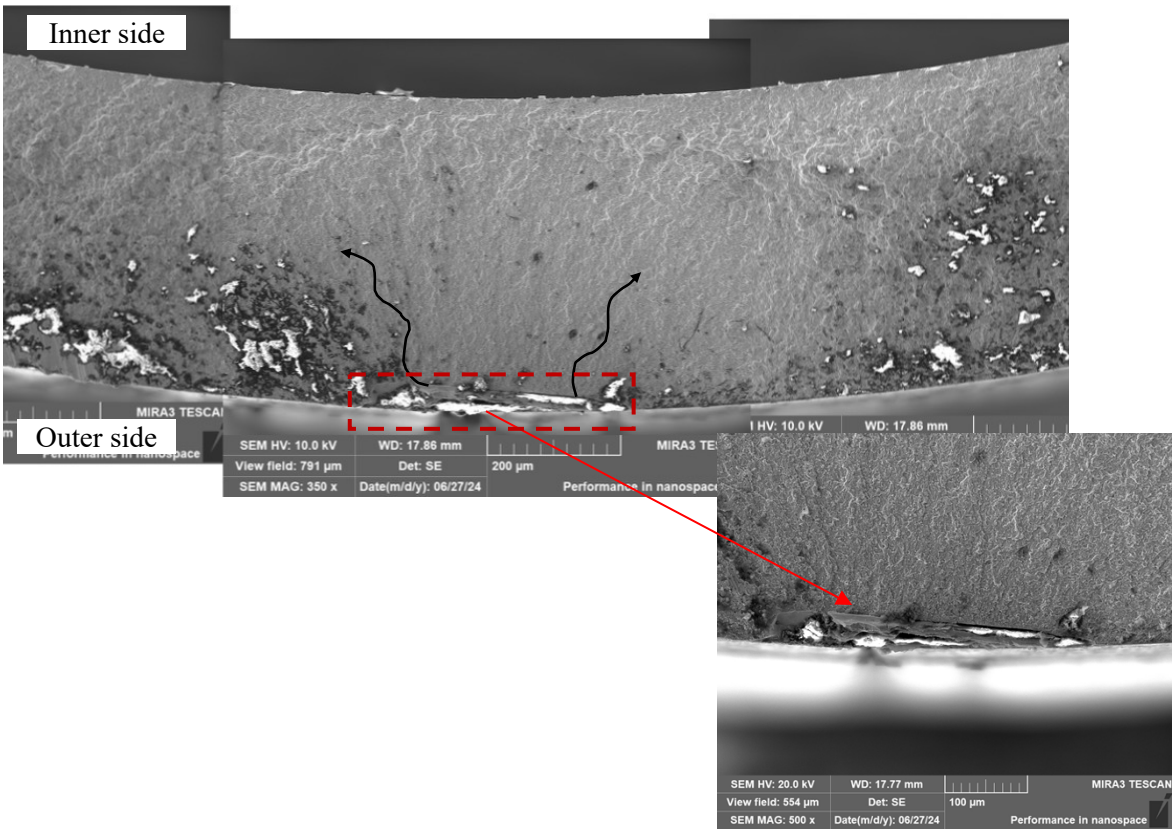


*Fig. 11. Fracture initiation site of sample H302. Insert shows a high magnification image of the crack initiation site. Black arrows indicate the direction of crack propagation from the initiation site.*

The FISs of samples H101, H103 and H301 were selected for further characterization using optical microscopy. The goal was to study the region underneath the crack initiation site to elucidate the influence of hydride phase formations in the fatigue initiation process. The sample preparation involved sectioning the sample at the fatigue initiation region and revealing the cross section along the thickness as shown in Fig. 12 (b) and (c). Both halves from the sectioning process were mounted side-by-side for metallographic characterization, as shown in Fig. 12 (e).

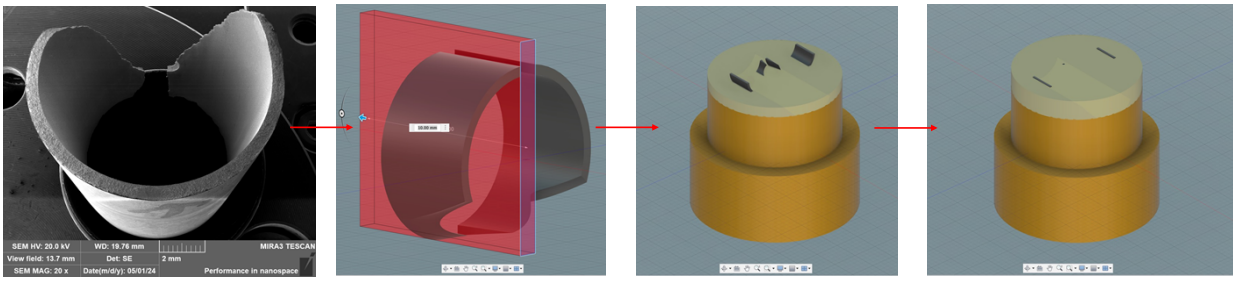

(a) (b) (c) (d)


(e)

*Fig. 12. Sample cutting and mounting steps for metallography - (a) fracture cross section from SEM analysis; (b) Schematic showing the axial cut made to open the fracture initiation site; (c) Schematic showing the two halves on a MET mount after slicing; (d) Schematic of the MET mount with the two halves in epoxy with the thickness along the initial fracture facing upwards; (e) The prepared MET mounts of samples H101, H103 and H301 ready for etching and imaging.*

The sample preparation involved polishing and etching the mounted samples. Three polishing pads at different polish settings were used as specified in Table 3. The etching procedure involved initially exposing the sample to an acid etchant of composition 19.4 mL $HNO_3$, 19.4 mL $H_2O_2$, and 1.2 mL HF, for 10 seconds, followed by two 10-second exposures to DI water solutions for washing away the etchant and preventing over-etching. The samples were then rinsed in isopropanol before being imaged.

*Table 3 Polishing procedures used in this study.*

| Serial No. | Polishing pad | Polishing time (min) | Force used on sample (N) | Polisher wheel rotation (rpm) |
|---|---|---|---|---|
| 1. | 9µm Allegro | 4 | 30 | 150 |
| 2. | 6µm LARGO | 4 | 15 | 150 |
| 3. | 3µm DAC | 4 | 30 | 150 |

Fig. 13 to Fig. 15 show the optical micrographs of paired cross sections near the fatigue crack initiations sites in H101, H103 and H301. The crack initiation site, OD and ID sides have been marked in the figures to highlight the sample's orientation prior to being sectioned. The distribution of hydrides was observed to be homogeneous in all samples and with no distinct hydride rims. The hydride platelet distributions within the cross sections are observed to be spread along the longitudinal direction of the cladding with a slightly higher concentration of hydrides distributed on the ID side, for all samples. At 1300 ppm of hydrogen, the distribution looked similar to what was expected at such hydrogen concentrations by Daum et al.[44] There was no clear indication of a higher hydride concentration near the crack tip, as observed Garlea et al. in a similar study looking at fatigue failure modes in hydrided Zry-4 plates.[45] However, there was an observed warping on the crack tip surface and around the edges of the specimen, which might have masked some of the features that were being probed for.

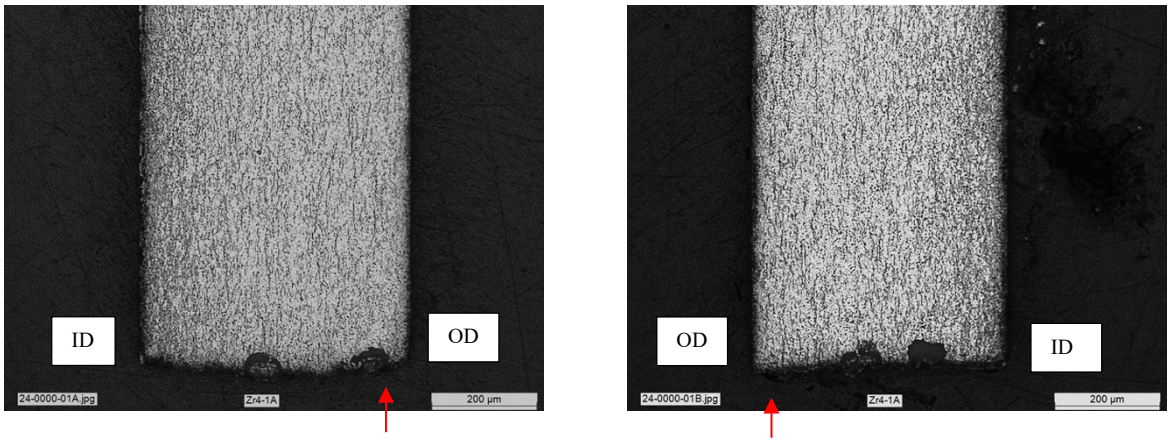


*Fig. 13. Metallographic images of the cross section along the fracture initiation site's thickness for sample H101 (FIS at OD); (a) & (b) show cross sections on either side of the cut.*

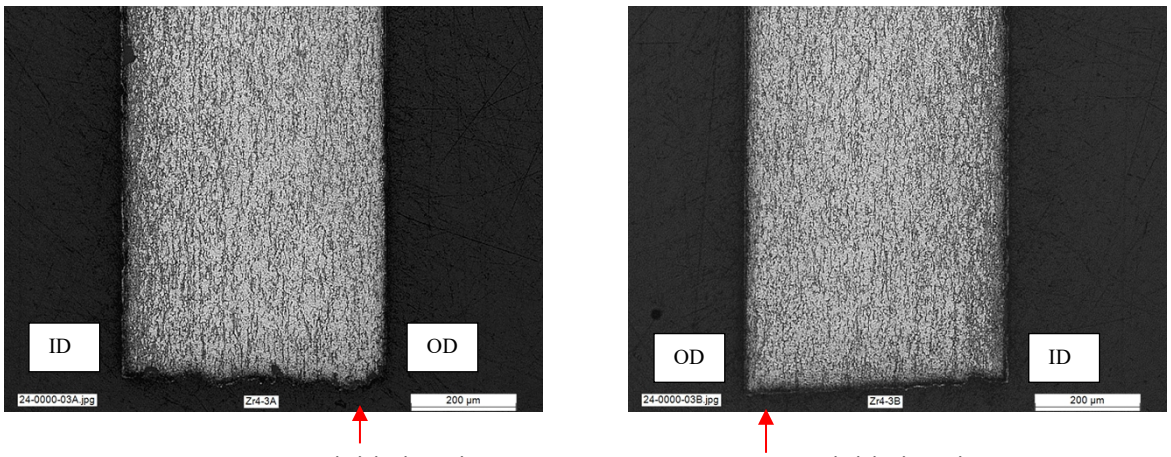


*Fig. 14. Metallographic images of the cross section along the fracture initiation site's thickness for sample H103 (FIS at OD); (a) & (b) show cross sections on either side of the cut.*

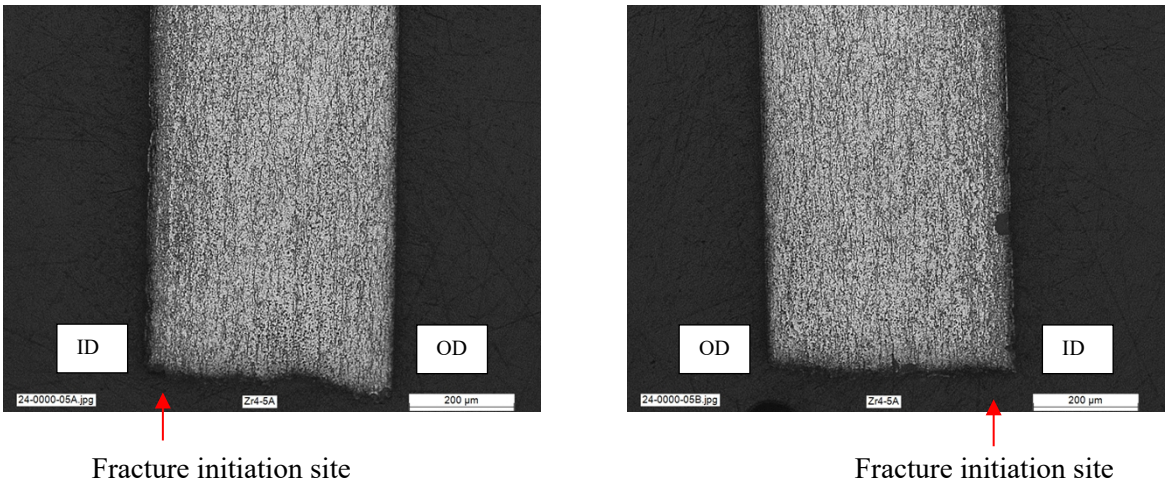

(a) (b)

*Fig. 15. Metallographic images of the cross section along the fracture initiation site's thickness for sample H301 (FIS at ID); (a) & (b) show cross sections on either side of the cut.*

## 5.3 Hydrogen Content Measurement

The total cladding hydrogen of specimens H101, H103, H301, H302 and H303 were measured using a LECO Model 836 analyzer in order to compare the hydrogen concentrations and further elucidate the difference in fatigue performance as a function of it. Thus, 2 mm sections were made under the fracture locations of all samples using a diamond saw and the sections were further cut down into four specimens for the LECO analysis. The analysis procedure involves system calibration with two standards – 502-891 & AR 649 with hydrogen concentrations of about 100 wt. ppm and about 200 wt. ppm, respectively. However, calibration standards beyond 200 wt. ppm were not available and using multiple AR 649 calibration standards for a single calibration measurement was impossible due to the system's allowable sample mass range. Hence, the calibration curves are extrapolated to encompass the high hydrogen levels about 1300 ppm) expected in the samples. A measurement uncertainty based on the standard deviation of four samples from each specimen is thus quoted along with the hydrogen values in Table 4. As seen from Table 4, H301 had one and H303 had two anomalous runs showing abnormally low H content. This was a result of the specimen falling out of the LECO sampling basket during loading. The calculated average and standard deviation for each sample subsets exclude these anomalous data points (shown in red in Table 4).

*Table 4. Average hydrogen content in the samples*

| Sample | Specimen mass (g) | Hydrogen concentration | Average Hydrogen (wt. ppm) | Hydrogen Std. Dev. |
|---|---|---|---|---|
| H101 | 0.0575 | 0.112% | 1280 | ± 0.0124% |
| | 0.0489 | 0.125% | | |
| | 0.0533 | 0.135% | | |
| | 0.0584 | 0.140% | | |
| H302 | 0.0510 | 0.131% | 1230 | ± 0.0112% |
| | 0.0536 | 0.118% | | |
| | 0.0390 | 0.134% | | |
| | 0.0489 | 0.110% | | |
| H103 | 0.0583 | 0.129% | 1310 | ± 0.0110% |
| | 0.0390 | 0.121% | | |
| | 0.0368 | 0.126% | | |
| | 0.0447 | 0.147% | | |
| H301 | 0.0249 | 0.000220% | 1280 | ± 0.0107% |
| | 0.0507 | 0.140% | | |
| | 0.0459 | 0.130% | | |
| | 0.0335 | 0.114% | | |

| | | | | |
|---|---|---|---|---|
| H303 | 0.0210 | 0.127% | 1240 | ± 0.00348% |
| | 0.0237 | 0.000832% | | |
| | 0.0343 | 0.122% | | |
| | 0.0248 | 0.00199% | | |

All fractured samples measured the same range of hydrogen concentrations with a mean value of 1268 ppm. H103 seems to have the higher hydrogen concentration among all samples with 1310 ppm. The LECO analysis highlights the importance of specific hydride structures in the cladding influencing mechanical behavior, even though the overall average hydrogen concentration is comparable.

# 6. DISCUSSIONS

The fatigue data provided herein indicate that the process of pre-hydriding can result in a dramatic improvement in the high-cycle fatigue performance (H104, H105, H106) where the endurance limit was measured to be at least 0.38% compared to previous measurements for AR and polished cladding, which were less than 0.28%. However, the observation of failure initiating on the ID when these H105 and H106 specimens were further tested at higher strain amplitude (H301, H303) is consistent with failure initiation sites in the AR and polished cladding. Because the defects size on the ID surface is unchanged by the pre-hydriding process, it would appear the pre-hydriding process has the potential to improve the fatigue performance of the cladding.

In contrast, the pre-hydrided specimens H101 and H103 tested at $\varepsilon_a$ = 0.32% and 0.41%, respectively, failed in less than 50,000 cycles. While the hydride levels in these specimens were similar to those in H104-H106, the failure initiation site was clearly on the OD surface rather than the ID surface. In addition, the low-cycle fatigue performance of H101 and H103 were degraded compared to the AR and polished cladding. However, the observation of OD failure on specimen H102 ($\varepsilon_a$ = 0.25%) when tested further at a higher strain amplitude (H302, $\varepsilon_a$ = 0.43%) suggests that the endurance limit observed in H102 is representative of these pre-hydrided OD-failure specimens. That is, that the endurance limit of these pre-hydrided specimens with OD failure is similar to the AR and polished condition.

Thus, it appears there are two populations of pre-hydrided fatigue performance that clearly correlate to failure initiation site. For the specimens with failure initiation on the OD, there appears to be a decrease in low-cycle fatigue performance compared to the AR and polished cladding but similar high-cycle fatigue. For the specimens with failure initiation on the ID, there is a possible improvement in low-cycle fatigue performance compared to the AR and polished cladding but a dramatic improvement in high-cycle fatigue performance.

The reasons for these observed differences are purely speculative at this time. It is suspected that the OD failures are caused by a very special hydride structure on the surface of specimens H101, H102/H302, and H103 that are not present in H104, H105/H301, and H106/H303, even though the samples all have similar hydrogen content. In this case, the surface hydride cracks earlier in the fatigue test resulting in degraded low-cycle fatigue performance. However, because specimen H102 reached the endurance limit at $\varepsilon_a$= 0.25% but failed on the OD at $\varepsilon_a$ = 0.43%, it appears the surface hydrides did not prematurely crack at $\varepsilon_a$= 0.25%.

The more difficult observation to explain is the improved performance of specimens H104, H105/H301, and H106/H303. In these samples, the pre-hydriding process appears to have delayed failure initiation on the ID compared to the AR and polished cladding. Because there is no change in the geometry of the ID surface defects, the only explanation is that the stress state around those defects is different in these pre-hydrided cladding specimens than in the AR and polished cladding. One explanation could be that

residual stresses near the ID surface of the AR and polished cladding are relieved during the pre-hydriding process making it more difficult to start a fatigue crack. In addition, once started the fatigue crack propagation may not be sensitive to the hydrogen content tested herein.

## 6.1 Fracture Initiation Site

A marked ε-N scatter plot with the fracture initiation site (FIS) is given in Fig. 16, which is based on Fig. 5 (b). For a given data group, for example, H301 to H303, the FIS at OC is located in the left side of the data group, suggesting a lower fatigue life. And those at ID correspond to a longer life. The observation of ID FIS for the pre-hydrided group reminisces that of ID FIS in the AR and polished data groups,[46] part of which are also marked. Therefore, it appeared that a longer fatigue life in the fatigue-treated pre-hydrided cladding tube was attained by suppressing the FIS at OD.

The OD FIS failure in the H302 manifests itself that the specimen H102 would be dominated by an ID FIS failure as well in the high cycle region. Same comment applies to the ID FIS failure in the H301 and H303 as to the H105 and H106. The deduced FIS type is also marked in Fig. 16 but with dotted outline.

Overall, the OD FIS data define a lower envelope, and all the ID FIS data are scattered above the envelope. The reason why FIS was retained at ID and shifted to OD in the pre-hydrided cladding was explained above, and the data are analyzed further in the following.

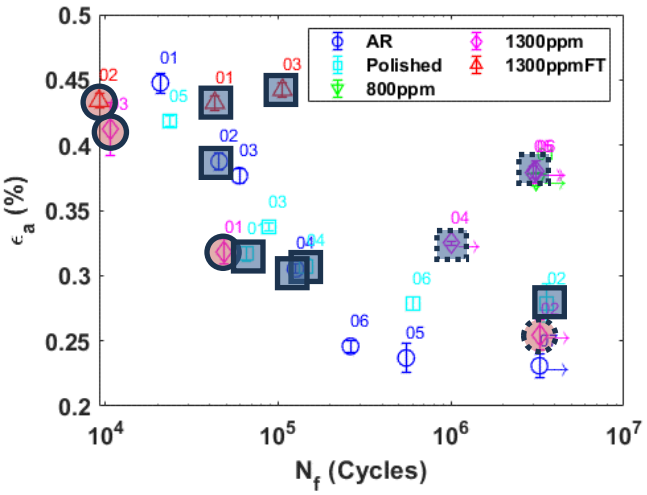


*Fig. 16 Marked strain as a function of number of cycles to failure. AR – as-received; 1300ppmFT- pre-hydrided to 1300 ppm and cycled to more than $3\times10^6$ cycle. Solid circle – fracture initiation site at OD, and solid square – fracture initiation site at ID. The marker with dashed outline indicates the FIS deduced based on the 1300ppmFT data.*

## 6.2 Hydrogen Content

For the failed pre-hydrided specimens, examination of ε-N scatter in Fig. 5 as a function of hydrogen contents did not reveal any correlation between the fatigue life and hydrogen content or that between the data pattern and hydrogen content. This occurred perhaps because of the small variation of hydrogen contents investigated. To obtain a better picture on the effect of hydrogen content on the fatigue, it may be necessary to re-examine 800 ppm group.

## 6.3 Fatigue Life

The O'Donnell-Langer (O-L) equation[47] relates the number of cycles to failure, $N_f$, to strain amplitude, as below:

$$\varepsilon_a = \frac{25}{\sqrt{N_f}} ln \frac{100}{100 - RA} + \varepsilon_e, \quad (11)$$

where $\varepsilon_a$ is the strain amplitude, *RA* is the reduction of area, and $\varepsilon_e$ is the fatigue limit or endurance limit, all in %. The O-L equation is effective in characterizing the fatigue response of materials in both low and high cycle regions, including characteristic fatigue limit. In the following, this equation is applied for the pre-hydrided cladding data to examine the effect of OD FIS and ID FIS by following the procedure established.[48-51] The pre-hydrided database was extended to include the repeated tests of un-failed specimens at the high strains. As a result, the H1 and H3 series data were sorted into the two FIS groups: the OD FIS includes H101 to H103, and H302; the ID FIS includes H104 to H106, H301 and H303. The results are given in Fig. 17 (a), and fitting parameters provided in Table 5. As expected, the curve fitting resulted in a lower value of RA and $\varepsilon_e$ for OD FIS group than that of ID FIS group. However, the difference is statistically insignificant.

The two FIS groups of data were pooled together, and the O-L curve fitting was carried out with the results shown in Fig. 17 (b) and Table 6 along with previous data.[41] It has been demonstrated that, compared to polished data, the RA of pre-hydrided cladding was reduced by 50% and $\varepsilon_e$ increased by 36%. The reduction in RA revealed by the fatigue data obviously agrees with the averaged decrease of RT tensile RA as summarized in Table 1. On the other hand, the fatigue limit can be related to the tensile property as well. For example, for the low and medium strength steels, the fatigue limit is about 50% of UTS.[48] The fatigue limit, $\sigma_e$, can be expressed in terms of strain fatigue limit, $\varepsilon_e$, and Young's modulus E as follows,

$$\sigma_e = E\varepsilon_e. \quad (12)$$

For the pre-hydrided cladding, a 28% reduction of E as shown in Fig. 6(a), and 36% increase in $\varepsilon_e$ would result in a fatigue limit nearly same as that of the polished cladding, about 98%. The insensitivity of fatigue limit revealed to pre-hydriding appears to correspond to the un-defined trend of UTS as a function of hydrogen content as shown in Table 1.

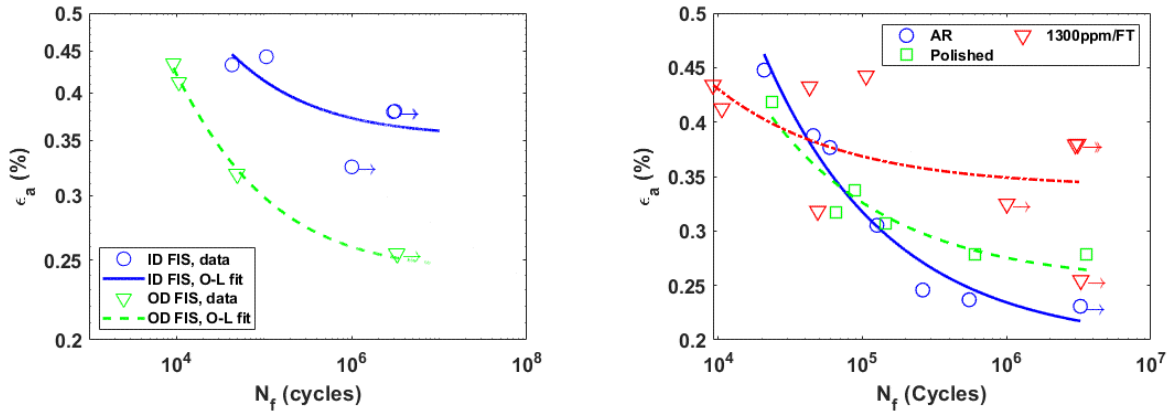


(a) (b)

*Fig. 17 (a) Strain as a function of number of cycles to failure based on failure mode. ID FIS - FIS at ID surface; same comment applied for OD FIS; H1 and H3 data were re-grouped according to the location of FISs. (b) Pooled strain data as a function of cycles to failure and O-L curve fitted lines. Solid line – As-received (AR); dashed line – Polished; dot-dashed line – Pre-hydrided to 1300 ppm and fatigue treated.*

*Table 5 O-L fitting parameters for pre-hydrided Zry4 cladding tubes*

| **Group** | **RA*** | **$\varepsilon_e^*$** |
|---|---|---|
| | % | % |
| ID FIS | 53.4 (26.9, 70.3) | 0.353 (0.324, 0.383) |
| OD FIS | 51.2 (49.3, 53.0) | 0.242 (0.235, 0.249) |

* The interval is for one standard deviation.

*Table 6 O-L curve-fitting parameters of pooled pre-hydrided data compared to those of as-received and polished Zry-4 data*

| **Group** | **RA*** | **$\varepsilon_e^*$** | **Refs.** |
|---|---|---|---|
| | % | % | |
| Pre-hydrided, 1300 ppm | 30.3 (12.7, 44.3) | 0.340 (0.310, 0.370) | This study |
| As-received | 78.5 (74.8, 81.6) | 0.196 (0.181, 0.211) | [41] |
| Polished | 60.8 (53.8, 66.8) | 0.252 (0.237, 0.267) | [41] |

* The interval is for one standard deviation.

# 7. SUMMARY AND FUTURE WORK

## 7.1 Summary

Fatigue testing was carried for 1300 ppm group at 5 Hz by using a recently-developed cyclic integrated reversible bending fatigue tester (CIRFT). The testing was conducted within strain amplitude range between 0.25% and 0.41% with number of cycles ranged from $1.06\times10^4$ to $3.27\times10^6$. Only two specimens, H101 and H103, were cycled to failure with fatigue lives of $1.06\times10^4$ at 0.41% and $4.90\times10^4$ at 0.32%, respectively. H102, H105, and H106 were selected in the second round of testing but with a higher strain amplitude near 0.43%. These specimens were finally cycled to failure in the repeated tests with fatigue lives ranged from $9.2\times10^4$ to $1.06\times10^5$ cycles.

- For the failed specimens, fatigue curves demonstrate that: 1) flexural rigidity decreased in general, and 2) hysteresis increased. H102 exhibited distinct behavior with a rising R curve while the hysteresis was largely flat with slightly a tendency of decrease with normalized number of cycles.
- In the high cycle region, the induced strain amplitudes for the pre-hydrided un-failed specimens H104 to H106 are higher than previous data of as-received and polished cladding. In the low cycle region, the fatigue life is lower than that of previous data at the similar strain amplitude.
- While the loss angles fall within the data zone of previous results, the pre-hydrided specimens displayed a Young's modulus much lower than other Zry-4 specimens tested including those of the as-received and polished. The decrease in the modulus due to pre-hydriding accounts for about 28%.
- The hydrides were revealed to be oriented along the longitudinal axis of cladding tube as expected. The size and spacing of hydrides remain to be characterized. A LECO procedure was also utilized to measure the hydrogen content near the fracture surface of the failed specimens. The measured hydrogen contents are within a tight margin of the nominal value.
- The fracture initiation sites were observed on both the ID and OD surfaces of cladding tubes. For a given data group, the FISs at OC are located in the left side of the fatigue data group, suggesting a lower fatigue life. And those at ID correspond to a longer fatigue life.
- For the pre-hydrided group, the RA based on O-L analysis was reduced by 50% and the strain fatigue limit increased by 36% compared to the polished cladding data.

## 7.2 Nest Steps

Several aspects can be focused on in near future.

- Tensile property data: This has been planned for the miniature tensile specimens, but it may need to be coordinated on the relevant issue like the tensile direction. Out-of-cell ASTM E8 testing may be pursued. The monotonic test of the CIRFT may be enabled.
- Additional fatigue data are needed to define the ε-N curve with sufficient confidence level. Although the 1300 ppm group is being investigated, the fatigue data with the intermediate hydrogen content like 800 ppm are needed for defining the trend.
- At high temperatures, the UTS of pre-hydrided Zry-4 generally declines with the increasing hydrogen content, which may result in the reduced fatigue limit. Thus, the fatigue performance of pre-hydrided Zry-4 at reactor temperatures remains to be explored.

## ACKNOWLEDGEMENTS

This research was sponsored by the US Department of Energy, Assistant Secretary for Nuclear Energy, as part of the Advanced Fuels Campaign Program under Contract No. DE-AC05-00OR22725 with the US Department of Energy.

Authors sincerely thank the colleagues at ORNL for their kind help on the work reported: David Wilson and Darren Loposser for instrumentation support, Lianshan Lin and Chanaka Ihala Gamaralalage for reviewing the manuscript and providing comments.

# REFERENCES

[1] J., Kearns Terminal solubility and partitioning of hydrogen in the alpha phase of zirconium Zircaloy-2 and Zircaloy-4. J. Nucl. Mater. 22(1967), 292–303

[2] Y., Yan, T., Graening, and A.T., Nelson, , Hydriding, oxidation, and ductility evaluation of Cr-coated Zircaloy-4 tubing. Metals, 12(2022), p.1998.

[3] J. H., Huang, and S. P., Huang, Effect of hydrogen contents on the mechanical properties of Zircaloy-4. J. Nucl. Mater., 208 (1994) 166-179.

[4] J. H., Kim, M.H., Lee, B.K., Choi, and Y.H., Jeong, Effects of oxide and hydrogen on the circumferential mechanical properties of Zircaloy-4 cladding. Nucl. Eng. Design, 236(2006), 1867-1873.

[5] M., Le Saux, J., Besson, S., Carassou, C., Poussard, and X., Averty, Behavior and failure of uniformly hydrided Zircaloy-4 fuel claddings between 25 C and 480 C under various stress states, including RIA loading conditions. Eng. Failure Analysis, 17(2010), 683-700.

[6] Z., Wang, U., Garbe, H., Li, R.P., Harrison, K., Toppler, A.J., Studer, T. Palmer, and G., Planchenault, Hydride precipitation and its influence on mechanical properties of notched and unnotched Zircaloy-4 plates. J. Nucl. Mater., 436(2013), 84-92.

[7] H. M. Tung, and T.C., Chen, Hydride-Induced Responses in the Mechanical Behavior of Zircaloy-4 Sheets. Metals, 14(2024), 177.

[8] H., Lee, K.M., Kim, J.S., Kim, and Y.S., Kim, Effects of hydride precipitation on the mechanical property of cold worked zirconium alloys in fully recrystallized condition. Nucl. Eng. Techno., 52(2020), pp.352-359.

[9] S.-C., Lin, M., Hamasaki, Y.-D., Chuang, The effect of dispersion and spheroidization treatment of δ zirconium hydrides on the mechanical properties of zircaloy, Nucl. Sci. Eng. 71 (1979) 251-266.

[10] J. B., Bai, C., Prioul, D., François, Hydride embrittlement in ZIRCALOY-4 plate: Part I. Influence of microstructure on the hydride embrittlement in Zircaloy-4 at 20°C and 350°C, Metall. Mater. Trans. A 25 (6) (1994) 1185-1197.

[11] R. J. H., Wanhill, The Fatigue of Zircaloy-2 Containing Zirconium Hydride. The University of Manchester (United Kingdom), 1968.

[12] J.-A. J., Wang, H., Wang, Y., Yan, R., Howard, and B., Bevard, High Burn-up Spent Fuel Vibration Integrity Study Progress Letter Report (Out-of-cell Fatigue Testing Development—Task 2.1), ORNL/ TM-2010/288, Jan. 2011.

[13] J.-A. J., Wang, H., Wang, T., Tan, H., Jiang, T., Cox, Y., Yan, Progress Letter Report on U-frame Test Setup and Bending Fatigue Test for Vibration Integrity Study (Out-of-cell Fatigue Testing Development—Task 2.2), ORNL/TM- 2011/531, January 2012.

[14] J.-A. J., Wang, H., Wang, T., Cox, Y., Yan, Progress Letter Report on U-Frame Test Setup and Bending Fatigue Test for Vibration Integrity Study (Out-of-cell Fatigue Testing Development—Task 2.3), ORNL/TM- 2012/417, August 2012.

[15] J.-A. J., Wang, H., Wang, T., Cox, C., Baldwin, Progress Letter Report on Bending Fatigue Test System Development for Spent Nuclear Fuel Vibration Integrity Study (Out-of-cell Fatigue Testing Development—Task 2.4), ORNL/TM- 2013/225, July 2013.

[16] H., Wang, J.-A. J., Wang, T., Tan, H., Jiang, T. S., Cox, R. L., Howard, B. B., Bevard, and M. E., Flanagan, Development of U-frame bending system for studying the vibration integrity of spent nuclear fuel, J. Nucl. Mater. 440 (2013) 201-213.

[17] J.-A. J., Wang, H., Wang, and T., Tan, Reversal Bending Fatigue Testing, US Patent, US 8,863,585 B2, Oct. 21, 2014.

[18] J.-A. J., Wang, H., Wang, B. B., Bevard, R. L., Howard, and M. E., Flanagan, Reversible bending fatigue test system for investigating vibration integrity of spent nuclear fuel during transportation, Packag. Transp. Storage Secur. Radioact. Mater. 25 (2014) 119-132.

[19] J.-A. J., Wang, H., Wang, H., Jiang, and Y., Yan, CIRFT Testing of High-burnup Used Nuclear Fuel Rods from Pressurized Water Reactor and Boiling Water Reactor Environments, ORNL/TM-2015/313, September 5, 2015.

[20] J.-A., Wang, H., Wang, H., Jiang, Y., Yan, FY 2016 Status Report: Documentation of All CIRFT Data including Hydride Reorientation Tests, ORNL/SR-2016/424, September 14, 2016.

[21] J.-A., Wang, H., Wang, B. B., Bevard, J. M., Scaglione, FY 2017 Status Report: CIRFT Data Update and Data Analyses for Spent Nuclear Fuel Vibration Reliability Study, ORNL/TM-2017/291, Oak Ridge National Laboratory, Oak Ridge, TN, Aug. 8, 2017.

[22] J.-A., Wang, H., Wang, Mechanical fatigue testing of high-burnup fuel for transportation applications, NUREG/CR-7198, Rev. 1/ ORNL/TM-2016/689, prepared for Office of Nuclear Regulatory Research, U.S. Nuclear Regulatory Commission, Oct. 2017.

[23] H., Wang, J.-A. J., Wang, and H., Jiang, Fatigue behavior of spent nuclear fuel rods in simulated transportation environment, Proc. ASME 2017 Pressure Vessels & Piping Conference, PVP2017, Waikoloa, Hawaii, July 16-20, 2017, PVP2017-65842.

[24] J.-A., Wang, H., Wang, H., Jiang, B., Bevard, High burn-up spent nuclear fuel transport reliability investigation, Nucl. Eng. and Design 330 (2018) 497-515.

[25] H., Wang, J.-A. J., Wang, R., Montgomery, B. B., Bevard, CIRFT Data Analysis for Sister Rods, ORNL/TM-2019/1451, Oak Ridge National Laboratory, Oak Ridge, TN, Oct. 2020.

[26] R., Montgomery, J.-A. J., Wang, H., Wang, B. B., Bevard, D., Skitt, and O., Martinez, Sister Rod Destructive Examinations (FY20), Appendix F: Cyclic Integrated Reversible-Bending Fatigue Tests, ORNL/SPR-2020/1780, Oak Ridge National Laboratory, Oak Ridge, TN, Nov. 2020.

[27] P., Cantonwine, B.B., Bevard, D., Skitt, Y., Sasikumar, O., Martinez, R., Montgomery, H., Wang, and J.A.J., Wang, Sister Rod Destructive Examinations (FY22) Appendix F: Cyclic Integrated Reversible-Bending Fatigue Tests, ORNL/TM-2022/2733. Oak Ridge National Lab., Oak Ridge, TN, January 13, 2023.

[28] H., Wang, J.-A.J., Wang, Bending testing and characterization of surrogate nuclear fuel rods made of Zircaloy-4 cladding and aluminum oxide pellets, J. Nucl. Mater. 479 (2016) 470-482.

[29] H., Wang, and J.A.J., Wang, Data Processing Package for Cyclic Integrated Reversible Bending Fatigue Testing, ORNL/TM-2021/2114, Oak Ridge National Lab., Oak Ridge, TN, Jul. 2021.

[30] B. J., Lazan, Damping of Materials and Members in Structural Mechanics, Pergamon Press, Oxford, 1968.

[31] W. T., Thomson, Theory of Vibration with Applications, Fourth Ed., Prentice Hall, New Jersey, 1993.

[32] H., Wang, T., Matsunaga, H.-T., Lin, and A.M., Mottern, Piezoelectric and dielectric performance of poled lead zirconate titanate subjected to electric cyclic fatigue, Smart Mater. Struct. 21 (2012) 025009.

[33] ASTM B353-12, Standard Specification for Wrought Zirconium and Zirconium Alloy Seamless and Welded Tubes for Nuclear Service (Except Nuclear Fuel Cladding), ASTM International, West Conshohocken, PA 19428

[34] Y., Yan, Private communications, Apr. 5, 2024

[35] Fourgeaud, S., Desquines, J., Petit, M., Getrey, C. and Sert, G., 2009. Mechanical characteristics of fuel rod claddings in transport conditions. Packaging, Transport, Storage & Security of Radioactive Material, 20(2), pp.69-76.

[36] ASTM Standard C1322–15, Standard Practice for Fractography and Characterization of Fracture Origins in Advanced Ceramics, Jul. 1, 2019.

[37] H., Wang, and A.A., Wereszczak, Effects of electric field and biaxial flexure on the failure of poled lead zirconate titanate, IEEE Trans. Ultras. Ferroelec. Freq. Contr., 55 (2008) 2559-2570.

[38] H., Wang, H.-T., Lin, and A.A., Wereszczak, Strength properties of poled lead zirconate titanate subjected to biaxial flexural loading in high electric field, J. Am. Ceram. Soc. 93 (2010) 2843-2849.

[39] Y., Murakami, and M., Endo, Effects of hardness and crack geometries on ΔKth of small cracks emanating from small defects, in: K.J. Miller, E.R. de los Rios (Eds.), The Behaviour of Short Fatigue Cracks, EGF Pub. 1, 1986, Mechanical Eng. Publications, London, pp: 275-293.

[40] Y., Murakami, and M., Endo, Effects of defects, inclusions and inhomogeneities on fatigue strength, Int. J. Fatigue 16(3) (1994) 163-182.

[41] H. Wang, P. Cantonwine, Y. Sasikumar, T. Graening, K. Linton, Fatigue behavior of Cr-coated zircaloy-4 cladding tubes for accident-tolerant fuel development under fully reversed cyclic bending, in review.

[42] H. M., Chung, R. S., Daum, J. M., Hiller, M. C., Billone, Characteristics of hydride precipitation and reorientation in spent-fuel cladding, in: G.D. Moan, P. Rudling (Eds.), Zirconium in the Nuclear Industry: Thirteenth International Symposium, ASTM STP 1423, ASTM International, 2002, pp. 561–582.

[43] S., Suresh, Fatigue of Materials, 2nd ed, Cambridge University Press, New York, NY. 1998.

[44] R. S., Daum, Y. S., Chu, A. T., Motta, Identification and quantification of hydride phases in Zircaloy-4 cladding using synchrotron X-ray diffraction, J. Nucl. Mater., 392 (2009), 453-463.

[45] E., Garlea, H., Choo, G. Y., Wang, P. K., Liaw, B., Clausen, D.W., Brown, J., Park, P. D., Rack, and E. A., Kenik. Hydride-phase formation and its influence on fatigue crack propagation behavior in a zircaloy-4 alloy. Metall, Mater, Trans, A 41 (2010): 2816-2828.

[46] Y., Sasikumar, Summary of fractography analysis conducted on coated, polished and as-received samples, Oak Ridge National Laboratory, unpublished, Jul. 1, 2024.

[47] W. J., O'Donnell, B. F., Langer, Fatigue design basis for zircaloy components, Nucl. Sci. Eng. 20 (1964) 1-12.

[48] R. I., Stephens, A., Fatemi, R. R., Stephens, and H. O., Fuchs, Metal Fatigue in Engineering. John Wiley & Sons, 2000.

[49] M., Nakatsuka, T., Kubo, Y., Hayashi, C. M., Eucken, and A. M., Garde, Fatigue behavior of neutron irradiated zircaloy-2 fuel cladding tubes, in C.M. Eucken, A.M. Garde (Eds.), Zirconium in the Nuclear Industry: Ninth Int. Symp., ASTM STP 1132, ASTM, 1991, pp. 230-245.

[50] J. H., Kim, M. H., Lee, B. K. Choi, and Y. H., Jeong, Deformation behavior of Zircaloy-4 cladding under cyclic pressurization, J. Nucl. Sci. Technol. 44 (2007) 1275-1280.

[51] ASTM E1823 – 23, Standard Terminology Relating to Fatigue and Fracture Testing, ASTM International, West Conshohocken, PA 19428, Feb. 1, 2023.